Chapter 10
Identifying Atmospheric Aerosols with Polarization Lidar

Kenneth Sassen

Abstract A variety of types of aerosol particles, both natural and human-made, are commonly suspended in the atmosphere. Different aerosol types have characteristic shapes, but basically fall into two categories: spherical and irregular. Haze and forest fire smoke particles are examples of the former, and desert dust and biogenic debris (e.g., pollen) of the latter. It is shown here that the capability of polarization lidar systems to sense the exact shape of particles makes it a powerful tool to remotely identify many types of aerosols. This is particularly important in the study of how aerosols may affect the properties of clouds.

Keywords: Aerosol backscattering, aerosol shape, polarization lidar

10.1 Introduction

Aerosols suspended in the atmosphere have a variety of impacts ranging from human health to climate change. Layers of aerosols directly affect the radiative balance of the Earth–atmosphere system through scattering and absorption, thus increasing the local solar albedo (potentially cooling the surface and heating the atmosphere), and indirectly by modifying cloud particle phase and size distribution. These indirect aerosol effects on climate are highly uncertain (IPCC 2001). As examples, indirect aerosol effects include changes in the cloud condensation nuclei concentration or type, which affects water cloud albedo and the likelihood of precipitation development, while the ability for some particles, like mineral dusts, to serve as ice nuclei that affect cirrus cloud formation and the phase of supercooled clouds. Because the source (i.e., chemical composition) of aerosols determines to a large degree their ability to interact with light and affect clouds, it is important to be able to remotely determine aerosol type even at considerable distances from their source.

Geophysical Institute, University of Alaska Fairbanks, 903 Koyukuk Drive, Fairbanks, Alaska 99775 USA 907-474-7845, 907-474-7290 (FAX)

Y.J. Kim and U. Platt (eds.), *Advanced Environmental Monitoring*, 136–142.

Fortunately, the polarization lidar technique (Sassen 2000, 2005) has the unique ability to discriminate between spherical and nonspherical particles, and thus determine unambiguously the thermodynamic phase of clouds as well as identify the type of atmospheric aerosols because of its sensitivity to exact particle shape. Spherical aerosols (e.g., haze and aqueous smoke particles) produce no change in the polarization state of backscattered light, whereas nonspherical particles can generate considerable depolarization depending on the exact particle shape and, to some extent, on particle size relative to the incident wavelength (Mishchenko and Sassen 1998). For example, Asian dust storm aerosols have a highly irregular shape (Okada et al. 2001) and typically generate linear depolarization ratios (δ, the ratio of the returned laser powers in the planes of polarization orthogonal and parallel to that transmitted) of about 0.2–0.3 (Murayama et al. 2001; Sassen 2002), which is similar to some cirrus ice crystal clouds. If the particle dimensions are smaller than the incident wavelength, reduced depolarization will be measured for a particular nonspherical particle. However, those aerosols most likely to affect cloud properties have dimensions similar to (visible and near-infrared) lidar wavelengths, indicating that multiple-wavelength depolarization measurements are especially useful and could provide particle size estimates (Sassen et al. 2001). Such data, especially when combined with Raman (Wandinger 2005) or high spectral resolution lidar (Eloranta 2005) data, are very promising for characterizing the type, composition, and size of aerosols.

10.2 The AFARS Dataset

Current research at the Arctic Facility for Atmospheric Remote Sensing (AFARS) involves three polarization lidars (at 0.532, 0.694, 1.06, and 1.574 μm wavelengths) to study clouds, aerosols, and their interactions, as well as a 94-GHz polarimetric Doppler radar and various visible and infrared radiometers. In support of Aqua and Terra satellite overpasses over AFARS (64.86° latitude and −147.84° longitude), regular remote sensing observations involving mainly the "turnkey" cloud polarization lidar (CPL) are being obtained. The CPL is based on a high power (1.5 J), 0.1 Hz, ruby (0.694 μm) laser transmitter, and a two-channel receiver using a 25-cm diameter telescope (Sassen et al. 2001). The current ~3.0-y AFARS CPL dataset (as well as earlier midlatitude data from Salt Lake City, Utah) can be viewed at http://corona.gi.alaska.edu/AFARS/. Below we provide typical CPL data from various aerosol types sampled at AFARS.

10.3 AFARS Polarization Lidar Aerosol Studies

Time-averaged (approximately 10–30 min) vertical CPL profiles of linear depolarization ratios and relative returned laser power for three distinct types of boundary-layer aerosols over Fairbanks are given in Fig. 10.1. In each case the

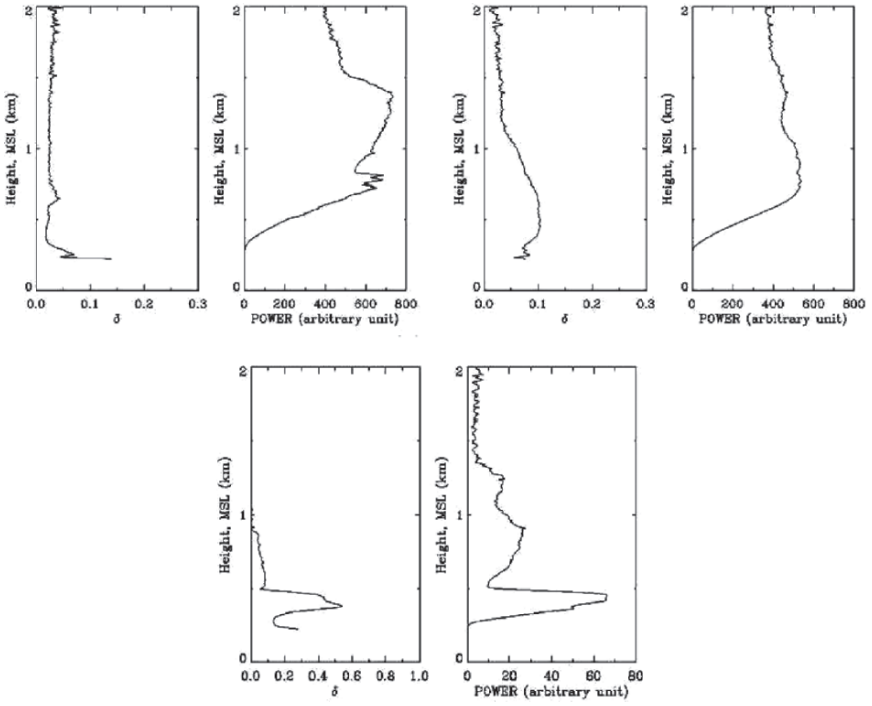

Fig. 10.1 Vertical profiles of CPL linear depolarization ratio δ and range-normalized relative returned laser power for three distinct types of Arctic aerosols, including Arctic haze (sampled on 3/31/04), tree pollen (5/14/04), and urban ice fog (12/24/04)

effect of the incomplete transmitter/receiver overlap is evident by the near-zero returned powers below about 300-m MSL (or ~100 m above the ground level). Also note that the δ values are what are referred to as the "total" depolarization ratios, because they are calculated from the sum of molecular and aerosol backscattering. Pure molecular backscattering yields δ of ~0.03 at the ruby wavelength.

At the upper left are profiles from an episode of Arctic haze, which, as in this case, often produces reduced horizontal visibility in winter and spring at high latitudes. The particles are aqueous droplets of ammonium sulfate solutions, derived photochemically from midlatitude air pollution. Because the particles are therefore spherical, near-zero depolarization is measured. Note that the peak returned power in the haze at ~1.4 km corresponds to the minimum δ value, slightly lower than the pure molecular value. (These droplets are too small and dispersed to generate any depolarization increase through the multiple scattering process.) Slight depolarization increases at lower levels are probably attributable to local urban pollution sources.

Next in Fig. 10.1 is shown the laser depolarizing effects of airborne biogenic debris, which are a common occurrence in the spring and summer at Fairbanks, and probably at many other locations as well. At the upper right are data from an occurrence

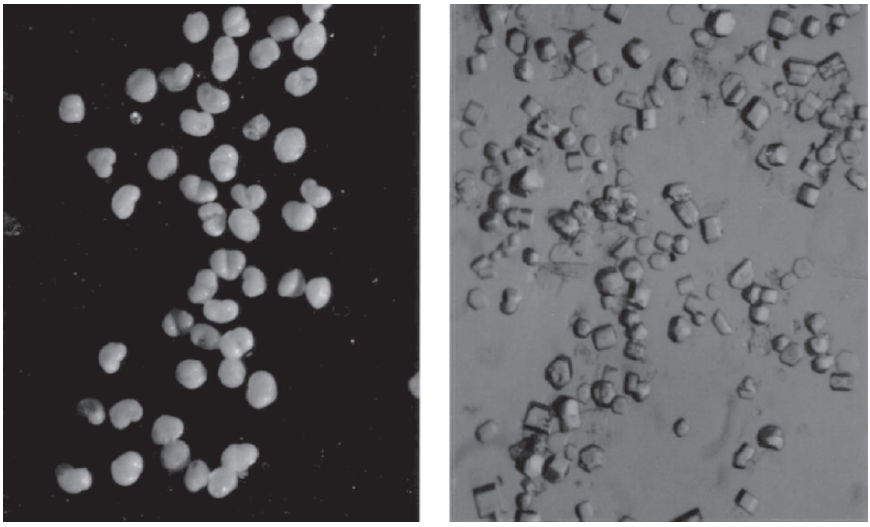

Fig. 10.2 Scanning electron microscope image of a) tree pollen (80x) at left collected during a solar corona display at Fairbanks, and at right, b) ice fog crystals (140x) showing a mixture of hexagonal and other habits (courtesy of Walter Tape)

of birch tree pollen grains. The presence of these relatively large (~20 μm) pollen during boreal forest green-out is indicated by the vividly colored solar corona. Although these particles are near-spherical in shape (see Fig. 10.2a), they are sufficiently nonspherical to generate $\delta \approx 0.1$. Cottonwood-type tree and firewood seeds, which are much larger than pollen grains and are often visible, swirling in the air, appear to generate a similar amount of depolarization.

Finally, shown at the bottom are profiles obtained from an ice fog generated at frigid temperatures (~−40°C and colder) from urban water vapor sources, particularly local power plants. The returned power peak at ~0.4 km height represents the ice fog layer, whereas the weaker signals aloft are probably from a mixture of Arctic haze and dispersed ice crystals. The relatively minute ice crystals usually display the typical hexagonal symmetry of naturally formed ice crystals, although unusual crystal forms are often observed in ice fogs (see Fig. 10.2b). These ice crystals generate δ up to 0.6, which is significantly higher than those values in cirrus clouds at similar temperatures (Sassen and Benson 2001).

We now provide height versus time CPL displays for additional types of aerosols studied at AFARS. Fig. 10.3a shows data obtained during an active forest fire season where a number of regional fires surrounding Fairbanks were burning. The result was a number of elevated smoke layers up to a height of ~8.0 km, as well as a dense smoke-filled boundary layer below ~4.5 km. Note the gravity waves present in the smoke layers. In contrast to the δ of ~0.3 in the broken cirrus cloud layer between 9.0 and 11.0 km height, the fresh smoke layers generate near-zero depolarization. This indicates that the aerosol was dominated by spherical aqueous droplets containing organic solutions liberated during the

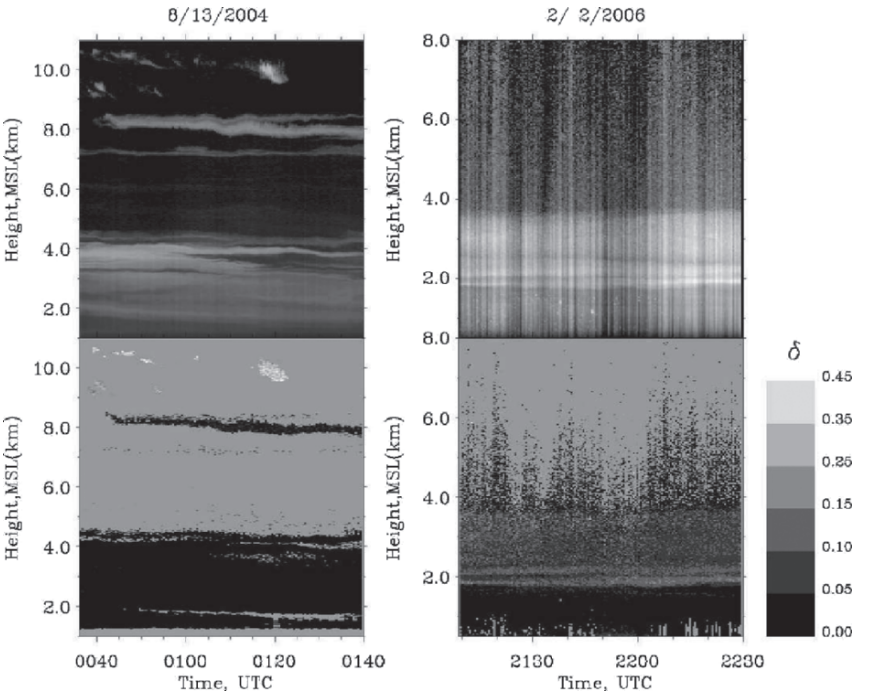

Fig. 10.3 Two examples of CPL height versus time displays of returned laser power (top, based on a logarithmic gray scale, where white is the strongest signal) and linear depolarization ratio (note δ scale at bottom right) for, (a) a smoky period at Fairbanks, and (b) a volcanic ash plume from the Augustine volcano south of Fairbanks

combustion process. In smoke layers that have aged and dried out, higher depolarization values are observed, presumably due to the crystallized remnants of evaporated droplets.

The final CPL aerosol study example is given in Fig. 10.3b, which shows a volcanic eruption cloud during late January 2006 from the Alaskan Augustine volcano. This volcano is ~850 km to the south of AFARS with a summit height of 1.26 km MSL, and weather conditions were briefly favorable in early February to transport the volcanic debris to our area. Volcanic aerosol transport models and satellite imagery confirm that the eruption cloud passed over AFARS at this time in the ~2.0 to 4.0 km height interval. (Note that the irregular returned power display at top was caused by variable ice fog plumes present below the beam cross-over point.) Although a fresh volcanic plume was previously observed by a Raman lidar (Pappalardo et al. 2004), these data are apparently the first laser depolarization measurements of a volcanic eruption plume in the troposphere. (However, Hayashida et al. (1984) appear to have sampled a lower stratospheric ash layer during the 2–5 month period following the El Chichón volcanic eruption in 1982, which yielded 0.10–0.15 δ values that are quite similar to those measured here.)

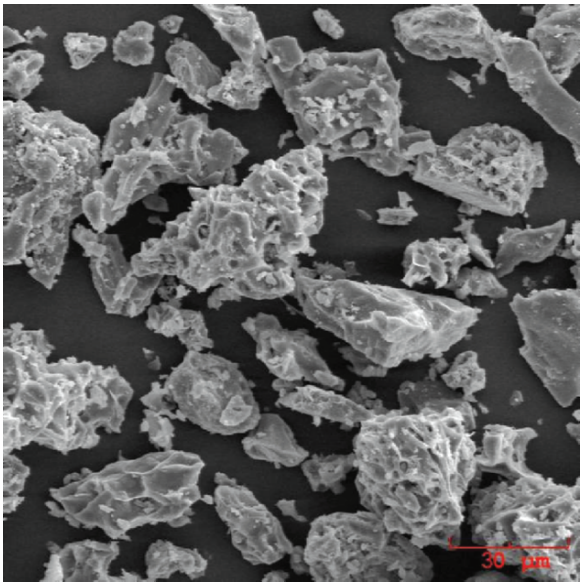

Fig. 10.4 Scanning electron microscope image (note that the sizes of three particles in the lower right corner are about 30 microns) of ash fallout from the late-January 2006 eruption of the Augustine volcano (courtesy of K. Dean of the Alaska Volcano Observatory). Because of the ~24-h transport time predicted by trajectory analysis to reach AFARS, the larger silica glass and feldspar crystals would have fallen out. Even the smallest particles have a highly irregular shape, however.

This amount of depolarization leaves little doubt that the aerosol is nonspherical, as is confirmed by the surface volcanic ash fallout sample shown in Fig. 10.4, which was collected 120 km from the volcano.

10.4 Conclusion and Outlook

We have shown several examples of ruby (0.694 µm wavelength) polarization lidar observations of various aerosols sampled in the Arctic region at AFARS in Alaska, including unique findings from an ash cloud from a nearby volcanic eruption. It is also interesting that boreal plants and trees produce floating pollen and seeds that generate noticeable amounts of laser depolarization. The sensitivity of the laser backscatter depolarization technique to exact particle shape means that there is a strong potential for identifying aerosol type (i.e., shape, composition, and relative size), especially when collected at two or more wavelengths and combined with quantitative lidar methods, which can separate out molecular scattering and determine backscatter-to-extinction ratios. We look forward at AFARS to a program involving depolarization measurements at four lidar wavelengths combined with new nitrogen Raman data to more fully evaluate the potential of

researching aerosols with lidar. Particularly promising for aerosol research is the 1.574-μm wavelength eye-safe scanning lidar, which has been designed to collect complete Stokes parameter, circular depolarization, and differential polarization data.

Acknowledgements This research is being supported by NASA grant # NNG04GF35G and NSF-MASINT (Measures and Signatures Intelligence) IRS 92-60000147.

References

Eloranta E.E. (2005), High spectral resolution lidar. In C. Weitkamp (Ed.), *Lidar*, (pp. 143–163). New York: Springer Press.

Hayashida S., Kobayashi A., and Iswasaka Y. (1984), Lidar measurements of stratospheric aerosol content and depolarization ratios after the eruption of El Chichón volcano: Measurements at Nogoya, Japan. *Geof. Int*., 23, 277–288.

IPCC (2001), *Climate change science: An analysis of some key questions. National Academy of Science*, retrieved from http://books.nap.edu/books/0309075742/html/.

Mishchenko M.I., and Sassen K. (1998), Depolarization of lidar returns by small ice crystals: An application to contrails, *Geophys. Res. Lett*., 25, 309–312.

Murayama T., et al. (2001), Ground-based network observation of Asian dust events of April 1998 in east Asia, *J. Geophys. Res*., 106, 18,345–18,360.

Okada O., Heintzenberg J., Kai K., and Qin Y. (2001), Shape of atmospheric mineral particles collected in three Chinese arid-regions, *Geophys. Res. Lett*., 28, 3123–3126.

Papapalardo G., et al. (2004), Raman lidar observations of aerosol emitted during the 2002 Etna eruption, *Geophys. Res. Lett.,* 31, L05120, DOI 10.1029/2003GL019073.

Sassen K. (2000), Lidar backscatter depolarization technique for cloud and aerosol research. In M. L. Mishchenko et al. (Eds.), *Light Scattering by Nonspherical Particles* (pp. 393–416). New York: Academic Press.

Sassen K. (2002), Indirect climate forcing over the western US from Asian dust storms, *Geophys. Res. Lett.,* DOI 10.1029/2001GL014051.

Sassen K., (2005), Polarization lidar. In C. Weitkamp (Ed.), *Lidar* (pp.19–42). New York: Springer Press.

Sassen K., and Benson S. (2001), A midlatitude cirrus cloud climatology from the Facility for Atmospheric Remote Sensing: II. Microphysical properties derived from lidar depolarization, *J. Atmos. Sci*., 58, 2103–2112.

Sassen K., Comstock J.M., Wang Z., and Mace G.G. (2001), Cloud and aerosol research capabilities at FARS: The facility for atmospheric remote sensing, *Bull. Am. Meteor. Soc*., 82, 1119–1138.

Wandinger U. (2005), Raman lidar. In C. Weitkamp (Ed.), *Lidar* (pp.241–271). New York: Springer Press.